Thermo-Mechanical and Damage Evolution at the Sidewall–Bottom-Corner Transition in 22MnB5 Steel during Hot Stamping

Yuanxiang Wang [1], Weilun Deng [1] and Hongxing Zheng [1,*]

https://doi.org/10.64486/m.66.2.10

[1] State Key Laboratory of Materials for Advanced Nuclear Energy, School of Materials Science and Engineering, Shanghai University, Shanghai 200444, China; wangyuanxiang@shu.edu.cn; dengweilun98@163.com
* Correspondence: hxzheng@shu.edu.cn

Type of the Paper: Article
Received: September 2, 2026
Accepted: September 24, 2026

Abstract: Hot stamping of 22MnB5 boron steel enables high-strength automotive components, but local deformation and damage may develop in geometrically constrained regions such as the sidewall–bottom-corner transition. A thermo-mechanically coupled DEFORM-3D finite element model was developed to examine local temperature, effective stress, effective plastic strain, and Damage under variations in die-entry temperature, punch speed, and friction coefficient. The deformation-sensitive region remained spatially stable, though its response magnitude varied with process conditions. Increasing die-entry temperature (750–850) °C reduced effective stress through thermal softening, with little change in final effective plastic strain and Damage. Increasing punch speed (50–150) mm·s^{-1} improved temperature retention and reduced effective stress, but increased effective plastic strain and Damage; increasing friction coefficient (0.3–0.7) substantially increased effective plastic strain and Damage with only limited effects on temperature and stress. Final Damage correlated strongly with final effective plastic strain (R^2 = 0.99, partly reflecting the cumulative NCL formulation) but showed a weaker correlation with final effective stress (R^2 = 0.62), indicating that instantaneous stress and accumulated Damage may exhibit different process-dependent trends and should therefore be considered jointly when assessing local deformation and damage accumulation.

Keywords: 22MnB5 boron steel; hot-stamp bending; finite element simulation; ductile damage; thermo-mechanical response

1. Introduction

Increasingly stringent requirements for energy efficiency, emission reduction, and crash safety have driven automotive body-in-white structures toward lightweighting and higher strength. 22MnB5 boron steel is widely used in safety-critical hot-stamped components because of its high specific strength, good toughness, and cost advantage. Its initial ferrite–pearlite microstructure transforms into a predominantly martensitic microstructure after austenitization, hot stamping, and in-die quenching [1]. Hot stamping combines high-temperature forming with in-die quenching, thereby reducing flow stress and forming load, suppressing springback, and enabling the production of complex, high-strength components. The cooling conditions during forming and quenching also influence the final microstructure and mechanical properties through phase transformation [2,3]. These characteristics have established 22MnB5 as a preferred material for structural components such as B-pillars, bumper beams, and rocker rails. Despite these advantages, hot stamping is a strongly coupled thermo-

mechanical process in which temperature, plastic deformation, frictional contact, and interfacial heat transfer evolve simultaneously. When these factors are not properly matched, deformation may localize and lead to excessive thinning, damage accumulation, and cracking. Seo *et al*. reported rapid thinning and fracture in the sidewalls of hot deep-drawn boron steel parts under tensile loading, with increased blank-holding force further promoting cracking [4]. Z. Tang *et al*. showed that the pre-forming path can substantially alter the thickness distribution of hot-stamped beam components [5]. These studies indicate that local deformation history and geometric constraints strongly influence hot-stamping failure. In components containing a sidewall–bottom-corner transition, the transition in deformation mode, combined bending–stretching deformation, and die-contact constraint together generate pronounced local variations in temperature, stress, strain, and damage. This region is therefore particularly relevant for examining localized thermo-mechanical and damage evolution.

The local response of this region is affected by die-entry temperature, punch speed, and interfacial friction coefficient. Die-entry temperature represents the actual blank temperature when the heated sheet enters the forming stage and contacts the tooling. Because of radiative and convective heat losses during transfer, it is generally lower than the furnace austenitization temperature. Industrial furnace austenitization is generally conducted at (850–950) °C [6], and the high-temperature deformation behavior of 22MnB5 is highly sensitive to temperature and strain rate [7]. Therefore, the actual die-entry temperature provides a more representative thermal boundary condition for the forming stage than the furnace set-point temperature. An excessively low die-entry temperature reduces thermal softening and may promote non-uniform deformation, whereas excessive furnace temperature or prolonged soaking can cause grain coarsening, oxidation, and coating degradation [8,9]. Beyond thermal effects, punch speed and friction coefficient influence the forming response through different but coupled mechanisms. Increasing punch speed reduces the time available for heat transfer from the blank to the die, thereby improving temperature retention, while simultaneously increasing the deformation rate and modifying the flow-stress response [10,11]. In contrast, friction primarily governs interfacial sliding and material feed-in and consequently affects forming load, strain distribution, and local thinning. Because hot-stamping friction is affected by lubrication, coating evolution, oxide scale, surface roughness, contact pressure, and temperature, its actual behavior is difficult to represent using a single constant coefficient [12–15]. In the sidewall–bottom-corner transition, increased frictional resistance may restrict material feed-in and promote local strain concentration. Thus, die-entry temperature, punch speed, and friction influence the local response through different pathways while remaining coupled through thermal softening, strain-rate effects, heat transfer, and deformation constraint, providing the basis for examining both individual parameter effects and representative two-factor combinations. It should also be noted that, in practical hot stamping, the substrate is commonly protected by Al–Si- or Zn-based coatings, which can modify interfacial friction and heat transfer and may introduce additional failure mechanisms such as coating cracking and liquid metal embrittlement (LME) [16–19]. However, the present finite element model considers uncoated 22MnB5 steel. The calculated Damage is therefore interpreted as a relative measure of plastic damage accumulation in the substrate rather than a direct prediction of coating-related failure or LME. These coating-related effects are beyond the scope of the present study.

Because hot stamping involves successive stages of heating, transfer, forming, and in-die cooling, experimental measurement of the complete local evolution of temperature, stress, strain, and damage at the same material location throughout forming remains difficult. Finite element simulation therefore provides an effective approach for tracking local thermo-mechanical histories and evaluating the influence of process parameters. Hu *et al*. predicted the location and onset timing of cracks during 22MnB5 hot stamping using a continuum damage mechanics model [20]. Zhou *et al*. established a damage-coupled unified viscoplastic constitutive model to predict the high-temperature forming limit [21]. B. Tang *et al*. developed a ductile fracture criterion and demonstrated its capability to describe fracture initiation and evolution under complex stress states [22]. These studies demonstrate the applicability of numerical approaches to hot-stamping deformation and damage analysis. Nevertheless, previous studies have generally emphasized global forming behavior, forming limits, final strength, or maximum thinning, whereas the coupled temporal evolution of temperature, stress, plastic strain, and damage at a common material location has received comparatively less attention. In

 https://doi.org/10.64486/m.66.2.10

particular, although the normalized Cockcroft–Latham (NCL) Damage parameter inherently represents accumulated damage through integration over plastic deformation, previous studies have not clearly established how the instantaneous stress response and the resulting accumulated damage evolve relative to each other at a common material location under different hot-stamping process conditions. More importantly, it remains unclear whether a reduction in the instantaneous or final stress response necessarily corresponds to a reduction in accumulated damage when temperature, deformation rate, and frictional constraint change simultaneously. This distinction is important because the stress state governing the instantaneous mechanical response and the deformation history contributing to damage accumulation may be affected differently by thermal softening, strain-rate effects, and local deformation constraint. Accordingly, the scientific focus of the present study is not simply to identify a mathematical lack of synchronism arising from the cumulative form of the NCL Damage parameter. Rather, it is to determine how different thermo-mechanical process parameters modify the pathways of instantaneous stress response and accumulated damage at the same material location, and whether these pathways remain coupled or become separated under different forming conditions. This provides a physical interpretation of the non-synchronous response by distinguishing the respective roles of the current stress state and deformation history, while recognizing that the cumulative NCL formulation also contributes to this behavior.

Motivated by this gap, the present study established a thermo-mechanically coupled finite element model of 22MnB5 hot-stamp bending using DEFORM-3D and tracked the local response at the sidewall–bottom-corner transition. The effects of die-entry temperature, punch speed, and friction coefficient were examined through individual parameter variations and representative two-factor combinations involving concurrent variation of two process parameters. These selected combinations were not designed as a full factorial scheme and therefore were not used to isolate or quantify formal statistical interaction effects; rather, they were used to examine whether the response characteristics identified from the single-factor analyses remain consistent under representative coupled process conditions. Temperature, effective stress, effective plastic strain, and the NCL-based Damage index were evaluated throughout forming to distinguish their respective response pathways and to clarify the relationship between instantaneous mechanical response and accumulated damage. The specific objectives were to: (1) characterize the local thermo-mechanical and damage response of the sidewall–bottom-corner transition under different process conditions and assess the stability of the deformation-sensitive region; (2) examine whether the response pathways associated with die-entry temperature, punch speed, and friction coefficient remain consistent under representative concurrent variations of two process parameters (these combinations were not used to quantify formal statistical interaction effects); and (3) examine the relationship between final effective plastic strain, effective stress, and accumulated damage, and determine whether changes in the instantaneous stress response necessarily correspond to changes in damage accumulation under different thermo-mechanical loading paths. By distinguishing the instantaneous mechanical response from the history-dependent damage response, the study aimed to provide a more physically informed interpretation of local damage evolution in geometrically constrained regions of hot-stamped 22MnB5 components.

2. Finite Element Model

2.1. Geometry, Mesh, and Boundary Conditions

The material simulated in this study was a 22MnB5 high-strength boron steel sheet with a thickness of 1.6 mm. The hot-stamped component had a channel-shaped cross-section (Figure 1a), with a bottom flat-section width of 24 mm, a sidewall height of 22.4 mm, and a bottom-corner radius of 2.4 mm. The relative positions of the blank, punch, and die, together with the principal forming dimensions, are shown in Figure 1b. The tooling geometry was constructed at a 1:1 scale according to the actual hot-stamping die, thereby reproducing the geometric constraints of the actual forming configuration.

Simulations were performed using DEFORM-3D (DEFORM-11). The blank was modeled as a deformable body, whereas the punch and die were treated as rigid bodies because this study emphasizes the thermo-

 https://doi.org/10.64486/m.66.2.10

mechanical response of the blank rather than elastic deformation of the tooling. In the actual process, the blank undergoes heating, transfer, forming, holding/cooling, and demolding. Because the present study focuses on the local response during forming and in-die cooling, the heating and transfer stages were represented by prescribing the blank temperature at die entry rather than explicitly simulating these stages. The forming stage and the subsequent holding/cooling stage at the bottom dead center were then simulated. A Coulomb friction model with a constant coefficient was employed to describe relative sliding between the blank and the punch/die; this simplification does not capture the friction evolution observed in actual hot stamping [23]. A constant interfacial heat-transfer coefficient of 10 $kW \cdot m^{-2} \cdot K^{-1}$ was prescribed for heat transfer between the blank and the tooling. The punch and die were maintained at a constant temperature of 25 °C to represent the water-cooled tooling condition. These thermal boundary conditions and the prescribed heat-transfer coefficient were kept constant throughout all simulations to isolate the effects of die-entry temperature (T), punch speed (v), and friction coefficient (μ). Variations in tooling temperature and interfacial heat-transfer coefficient were not considered in the present parametric analysis. The die was fixed, while the punch moved toward the die at a prescribed velocity.

The blank, punch, and die were discretized using tetrahedral solid elements, resulting in 48,084, 40,133, and 44,225 elements, respectively (Figure 1c,d). During the development of the numerical model, a mesh-sensitivity assessment was performed at the representative 750 °C–100 $mm \cdot s^{-1}$–μ = 0.5 condition by refining the sidewall–bottom-corner transition and adjacent sidewall. The local element size was further reduced across three refinement levels (Mesh I–III) to evaluate the sensitivity of the effective plastic strain and Damage at point P. The difference between Mesh I and Mesh II was relatively pronounced (6.73 % for effective plastic strain and 3.95 % for Damage), whereas further refinement from Mesh II to Mesh III reduced the changes to 2.97 % and 0.48 %, respectively, both below 5 %, indicating that Mesh II provides a sufficiently converged local response within the investigated refinement levels. The corresponding refinement levels, local element sizes, and responses at point P are summarized in Table 1, and Mesh II was adopted for the subsequent simulations. The same mesh configuration, local-refinement strategy, and numerical settings were used for all other process conditions to maintain consistent spatial resolution and limit mesh-related variations in the comparison.

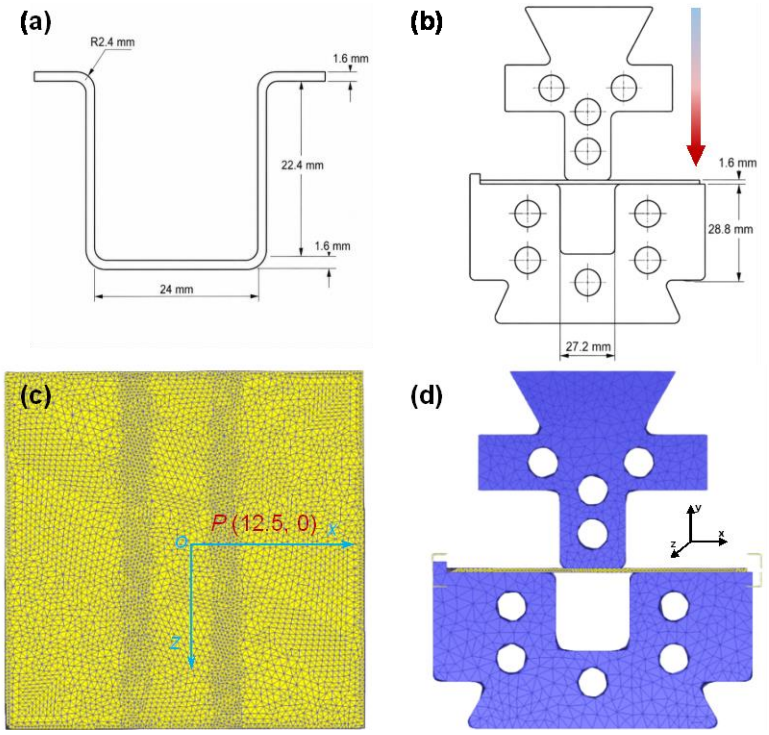


Figure 1. Dimensions of the simulated hot-stamping component (a); relative positions of the punch, die, and blank with corresponding forming dimensions (b); mesh discretization of the blank (c); and overall mesh discretization of the punch–die–blank assembly (d)

https://doi.org/10.64486/m.66.2.10

Table 1. Effect of local mesh refinement on effective plastic strain and Damage at point P (750 °C–100 mm·s^{-1}–μ = 0.5)

Mesh	Size ratio to element outside window	Local element size mm	Effective plastic strain	Damage
Mesh I	0.6	0.61–1.21	0.505	0.430
Mesh II (adopted)	0.5	0.51–1.00	0.471	0.413
Mesh III	0.4	0.40–0.81	0.485	0.411

2.2. Temperature-Dependent Material Parameters and Constitutive Model

22MnB5 undergoes substantial temperature variation during hot stamping, and its thermal and mechanical responses are strongly temperature dependent. Therefore, temperature-dependent material properties were adopted rather than constant values. The required thermophysical and mechanical parameters were calculated using JMatPro, a thermodynamic and materials-property calculation software, based on the chemical composition given in Table 2 and were subsequently implemented in DEFORM-3D as temperature-dependent material data. The temperature-dependent thermophysical properties included thermal conductivity, specific heat capacity, density, and Young's modulus (Figure 2). Thermal conductivity generally decreased with increasing temperature before increasing again at higher temperatures, while specific heat capacity exhibited a pronounced variation within the temperature range associated with phase transformation. Density decreased progressively with temperature, and Young's modulus decreased continuously, reflecting the reduced stiffness of the steel at elevated temperatures. These properties were used to describe heat conduction, thermal storage, and the temperature-dependent mechanical response of the blank during forming.

Table 2. Chemical composition of 22MnB5 steel / wt.%

C	Si	Mn	S	P	Cr	Ni	Mo	B	Al	Ti	Cu	V	Fe
0.23	0.25	1.35	0.006	0.015	0.19	0.028	0.04	0.003	0.04	0.03	0.016	0.004	bal.

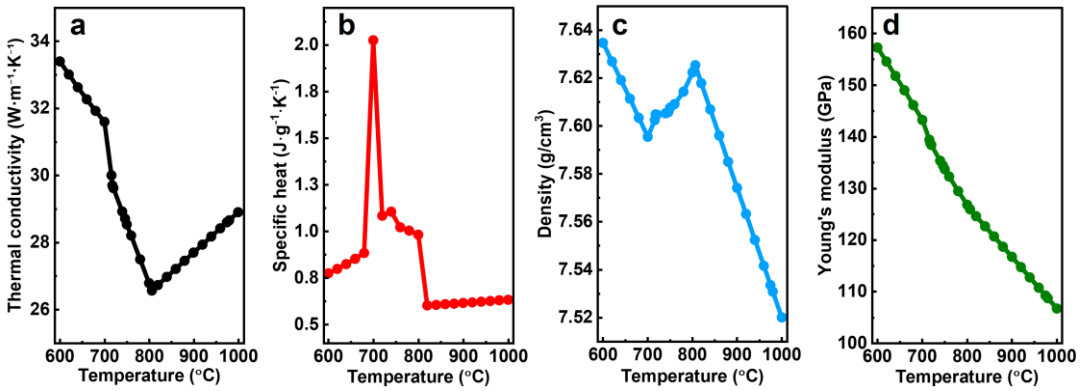


Figure 2. Temperature-dependent thermophysical parameters of 22MnB5 high-strength steel calculated using JMatPro software: thermal conductivity (a); specific heat (b); density (c); Young's modulus (d)

In addition to these thermophysical properties, the high-temperature flow behavior of 22MnB5 was described using flow-stress data calculated by JMatPro at a nominal strain rate of 0.001 s^{-1}. The corresponding true stress–strain curves are shown in Figure 3. As temperature decreased, the flow stress increased, whereas increasing temperature shifted the flow curves toward lower stress levels, demonstrating pronounced thermal softening. Strain hardening was also observed over the investigated strain range.

To represent the temperature- and strain-rate-dependent flow behavior in the numerical model, an Arrhenius-type hyperbolic-sine constitutive relationship was adopted:

$$\dot{\varepsilon} = A[\sinh(\alpha\bar{\sigma})]^n \exp\left(-\frac{\Delta H}{RT_{abs}}\right) \quad (1)$$

https://doi.org/10.64486/m.66.2.10

where $\dot{\varepsilon}$ is the strain rate (s^{-1}), $\bar{\sigma}$ is the von Mises effective stress (MPa), T_{abs} is the absolute temperature (K), and A, α, n, ΔH, and R are the material constants, namely, the pre-exponential factor (1.412×10^{10} s^{-1}), stress scale parameter (0.0043105 MPa^{-1}), stress exponent (7.9285), thermal deformation activation energy (154,985 $J \cdot mol^{-1}$), and gas constant (8.3145 $J \cdot mol^{-1} \cdot K^{-1}$), respectively. The general applicability of an Arrhenius-type formulation to the high-temperature deformation of 22MnB5 is supported by independent experimental studies. Zhou *et al*. [24] conducted hot tensile tests on 22MnB5 at (700–900) °C and strain rates of (0.01–10) s^{-1} and established a strain-compensated Arrhenius-type constitutive equation, supporting the applicability of this formulation to 22MnB5 under hot-stamping-relevant conditions. Tungtrongpairoj *et al*. [25] reported high-temperature deformation data for boron-alloy steel at 1000 °C and 0.001 s^{-1}, with flow-stress levels of the same order of magnitude as those derived from JMatPro in the present study. This comparison is considered only a supplementary consistency check because the temperature is outside the principal range investigated here and the strain rate corresponds to the nominal rate used for the JMatPro data. These literature results support the general applicability of the constitutive framework but do not independently validate the specific constitutive parameters derived from the present JMatPro data.

The transient temperature field in the blank was then governed by the heat-conduction equation:

$$\rho C_p \frac{\partial T}{\partial t} = \nabla \cdot (k \nabla T) + Q \tag{2}$$

where ρ is density, C_p is the specific heat at constant pressure, T is temperature, k is thermal conductivity, and Q is the volumetric heat source term. In the present model, the volumetric heat source in Eq. (2) was assumed to arise solely from plastic work dissipation, *i.e.*, $Q = Q_p$, expressed as:

$$Q_p = \eta \bar{\sigma} \dot{\varepsilon}_p \tag{3}$$

where η is the Taylor–Quinney coefficient, representing the fraction of plastic work converted into heat, which was set to 0.9, the default value used in DEFORM-3D, $\bar{\sigma}$ is the von Mises effective stress, and $\dot{\bar{\varepsilon}}_p$ is the effective plastic strain rate. Together with the temperature-dependent material properties and the prescribed blank–tool thermal boundary condition, these equations were used to calculate the transient thermal response during hot stamping.

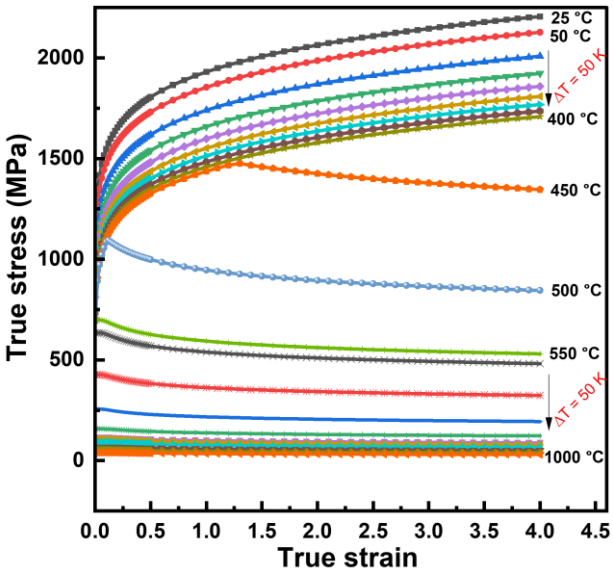


Figure 3. True stress–strain curves of 22MnB5 high-strength steel at different temperatures calculated using JMatPro

2.3. Ductile Damage Model

To evaluate the relative accumulation of ductile damage during hot stamping, the NCL damage model implemented in DEFORM-3D was employed:

https://doi.org/10.64486/m.66.2.10

$$D_{NCL} = \int_0^{\bar{\varepsilon}_p} \frac{\sigma_{max}}{\bar{\sigma}} d\bar{\varepsilon}_p \quad (4)$$

where D_{NCL} is the dimensionless NCL Damage value, σ_{max} is the maximum principal stress, $\bar{\sigma}$ is the von Mises effective stress, $\bar{\varepsilon}_p$ is the accumulated effective plastic strain, and $d\bar{\varepsilon}_p$ is the increment of effective plastic strain. The NCL formulation integrates the tensile component of the local stress state over the accumulated plastic deformation history. Therefore, D_{NCL} was used in this study as a dimensionless relative indicator for comparing the tendency for local damage accumulation among different process conditions. It was not used as a direct fracture criterion or as a quantitative prediction of crack initiation. Because no fracture experiments were performed to calibrate a critical NCL value for the present material and forming conditions, no critical Damage threshold is assigned in this study.

2.4. Simulation Scheme and Evaluation Point

A two-stage simulation scheme was designed to distinguish the individual response characteristics of the three process parameters and to examine their response under representative concurrent variations. In the first stage, a control-variable approach was used to examine the effects of die-entry temperature, punch speed, and friction coefficient separately. For the die-entry temperature group, the punch speed and friction coefficient were held constant at 50 mm·s^{-1} and 0.5, respectively, while the die-entry temperature was varied among 750 °C, 800 °C, and 850 °C. The punch-speed group followed the opposite arrangement: die-entry temperature and friction coefficient were fixed at 750 °C and 0.5, respectively, and the punch speed was varied among 50, 100, and 150 mm·s^{-1}. In the friction group, the die-entry temperature (750 °C) and punch speed (100 mm·s^{-1}) were kept constant, and only the friction coefficient was varied, taking values of 0.3, 0.5, and 0.7. In the second stage, three representative two-factor combination groups were considered to examine the response under concurrent variation of two parameters. The temperature–speed group fixed the friction coefficient at 0.5 and comprised three combinations: (750 °C, 50 mm·s^{-1}), (800 °C, 100 mm·s^{-1}), and (850 °C, 150 mm·s^{-1}). With the punch speed held at 100 mm·s^{-1}, the temperature–friction group examined (750 °C, 0.3), (800 °C, 0.5), and (850 °C, 0.7). The third group, speed–friction, was defined at a fixed die-entry temperature of 800 °C, spanning (50 mm·s^{-1}, 0.3), (100 mm·s^{-1}, 0.5), and (150 mm·s^{-1}, 0.7). These selected combinations were intended to represent concurrent process variations rather than a full factorial design; consequently, the second-stage simulations were used to examine the consistency of response trends under coupled process conditions, rather than to isolate or quantitatively determine formal statistical interaction effects. The first stage was used to identify the characteristic response to each individual parameter, whereas the second stage was used to examine whether these response trends remained consistent under concurrent variation of two parameters.

The sidewall–bottom-corner transition region was selected as the region of interest because it undergoes combined bending, stretching, contact constraint, and material-flow reorientation. This region was first identified from preliminary inspection of the spatial distributions of the deformation-related and damage-related variables under representative process conditions, which suggested localized mechanical and damage responses near the sidewall–bottom-corner transition; this spatial pattern is subsequently confirmed and quantified in Section 3.1 (Figures 4, 6, and 8). A Lagrangian material tracking point, denoted as P, was predefined on the blank at the initial coordinates (x = 12.5 mm, z = 0 mm). Point P was selected as a representative material location within this geometric transition zone, rather than according to the maximum Damage obtained in any individual simulation, and the same spatial pattern noted above consistently identifies this region as the principal deformation-sensitive zone under the investigated forming conditions. Accordingly, the quantitative analysis at P is used to characterize process-dependent trends and relative changes in the local response, rather than to assign a universal or absolute value to the entire transition region. The same material point was tracked throughout all simulations to provide a consistent reference for comparing the local thermo-mechanical and Damage responses under different process conditions. The response histories at point P were plotted against punch stroke rather than physical time, because punch stroke provides a common process coordinate for comparing simulations conducted at different punch speeds. The present analysis focuses on the forming stage: although the subsequent holding/cooling stage was included in the simulation setup, all

https://doi.org/10.64486/m.66.2.10

quantitative comparisons in Sections 3.1 and 3.2 refer to values at the end of the forming stroke, before holding/cooling. Temperature, effective stress, effective plastic strain, and NCL Damage were selected as the primary response variables to characterize the local thermal state, instantaneous mechanical response, accumulated plastic deformation, and damage evolution, respectively. Contour plots were used to identify the spatial distribution of these variables, and the histories at P were used for quantitative comparison among the investigated process conditions.

3. Results and Discussion

3.1. Effects of Single-Factor Process Parameters

Based on the finite element simulation scheme described above, this section examines how die-entry temperature, punch speed, and friction coefficient individually modify the local thermo-mechanical and damage response of 22MnB5 during hot-stamp bending. As defined in Section 2.3, the Damage values reported below are used only for relative comparison among the investigated conditions. Figures 4, 6, and 8 show the contour distributions of temperature, effective stress, effective plastic strain, and Damage for the three single-factor groups, while Figures 5, 7, and 9 quantify the corresponding response histories at point P as a function of punch stroke. Figure 4(a)–(c) presents the simulated fields at die-entry temperatures of 750, 800, and 850 °C, respectively. Increasing the die-entry temperature raises the overall temperature of the formed part and expands the high-temperature region, while the lower sidewall and sidewall–bottom-corner transition remain comparatively cooler than the surrounding material. The effective stress in the main sidewall region decreases with increasing die-entry temperature, and the high-stress region becomes progressively less extensive and more localized near the lower sidewall edge and corner. By comparison, the spatial distributions of effective plastic strain and Damage exhibit only minor changes, with their high-value regions remaining concentrated in the mid-to-lower sidewall and sidewall–bottom-corner transition.

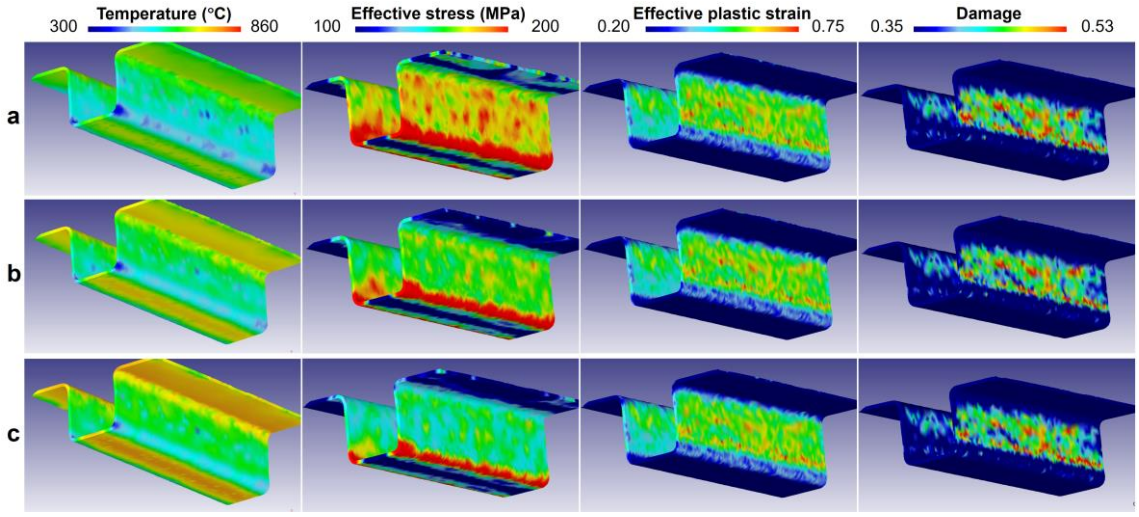


Figure 4. Effect of die-entry temperature on the thermo-mechanical response and damage distribution of the 22MnB5 hot-stamped component at a punch speed of 50 mm·s^{-1} and a friction coefficient of 0.5: (a) 750 °C; (b) 800 °C; (c) 850 °C

The corresponding histories at point P are shown in Figure 5. The temperature decreases continuously with punch stroke under all three conditions and reaches approximately 535 °C, 562 °C, and 596 °C at the end of forming for initial temperatures of 750 °C, 800 °C, and 850 °C, respectively. The corresponding temperature reductions are approximately 215 °C, 238 °C, and 254 °C. Although the absolute temperature drop becomes larger at higher die-entry temperature, the temperature at point P remains consistently higher throughout the forming process when the initial temperature is higher. The effective stress decreases with increasing die-entry temperature, consistent with the enhanced thermal softening of 22MnB5 at elevated temperatures. However,

https://doi.org/10.64486/m.66.2.10

the final effective plastic strain remains approximately 0.41, while the final Damage varies only within approximately 0.32–0.33. These results indicate that, within the investigated range of (750–850) °C, increasing the die-entry temperature primarily changes the thermal state and instantaneous stress response at point P, while exerting comparatively limited influence on the magnitude of deformation localization. This trend is broadly consistent with the experimental forming-limit results reported by Zhang *et al*. for 22MnB5, who used high-temperature biaxial tests with full-field DIC strain measurement and found that the forming-limit curve (FLC) and fracture forming-limit curve (FFLC) varied only modestly with temperature and strain rate over (750–850) °C and (0.02–0.5) s^{-1}, indicating that the temperature sensitivity of flow stress does not necessarily translate into a pronounced change in forming-limit strain [26] (Note: FLC/FFLC are necking/fracture-limit indices, whereas effective plastic strain and Damage here are local field responses—only a qualitative comparison is intended).

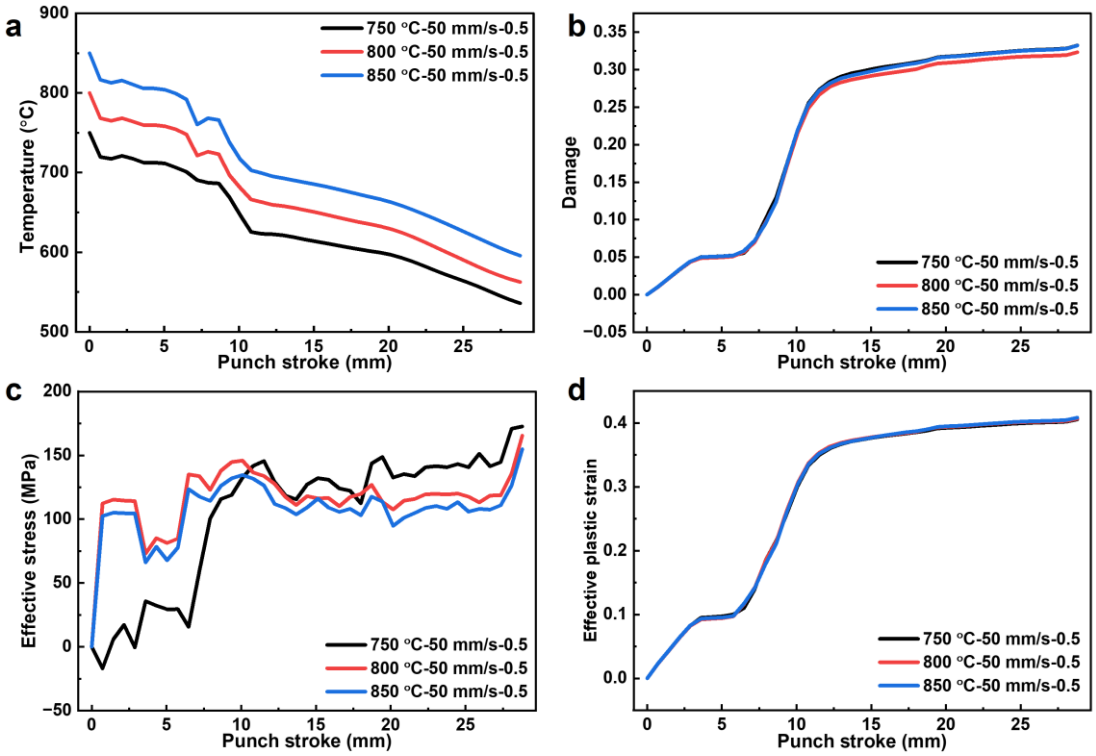


Figure 5. Evolution of temperature, Damage, effective stress, and effective plastic strain at point P with punch stroke under different die-entry temperatures (750 °C, 800 °C, and 850 °C) at a punch speed of 50 mm·s^{-1} and a friction coefficient of 0.5: (a) temperature; (b) Damage; (c) effective stress; (d) effective plastic strain

In contrast to die-entry temperature, punch speed introduces a pronounced thermal-retention and forming-time effect. Figure 6(a)–(c) shows the results obtained at punch speeds of 50 mm·s^{-1}, 100 mm·s^{-1}, and 150 mm·s^{-1}, respectively. As the punch speed increases, the overall temperature of the formed part increases and the low-temperature region becomes less extensive, indicating reduced heat loss from the blank to the tooling during the shorter forming period. This is consistent with reports for 22MnB5 hot stamping by He *et al*., who found that higher punch speed reduces heat loss during forming and keeps the blank at a higher temperature at fracture [27], and by Ganapathy *et al*., who showed for 22MnB5 automotive B-pillars that lower forming speeds prolong blank–die heat transfer and produce a more pronounced temperature drop [28]. The high-stress region also becomes less extensive and remains concentrated near the lower sidewall edge and corner. The locations of the high-effective-plastic-strain and high-Damage regions remain broadly unchanged, whereas their spatial extent becomes more pronounced with increasing punch speed. The same authors [27] further reported that higher punch speed raises the effective plastic strain rate and widens strain-rate

 https://doi.org/10.64486/m.66.2.10

differences among deformation zones in 22MnB5 hot stamping, promoting more non-uniform plastic deformation — consistent with the trend observed here.

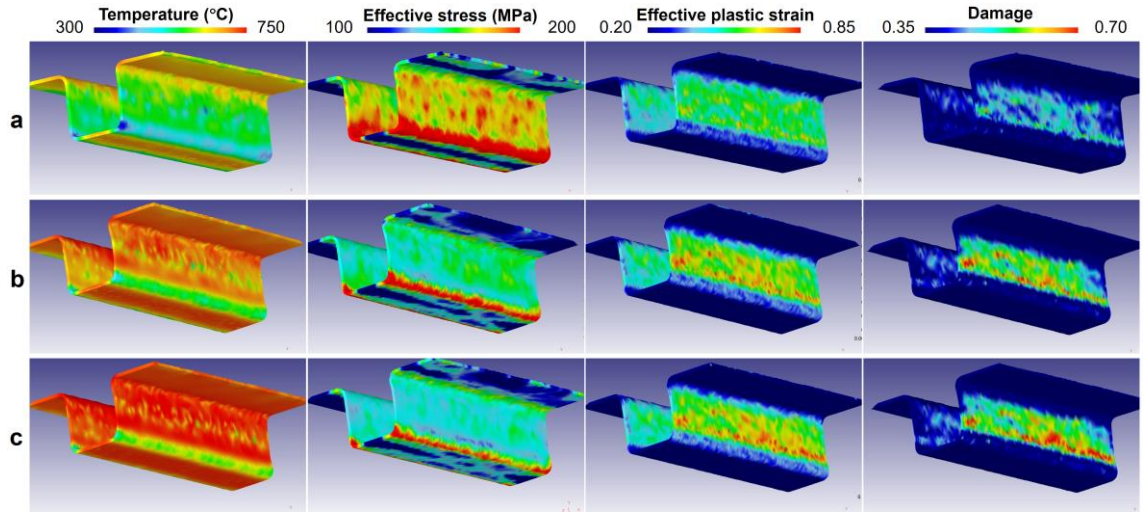
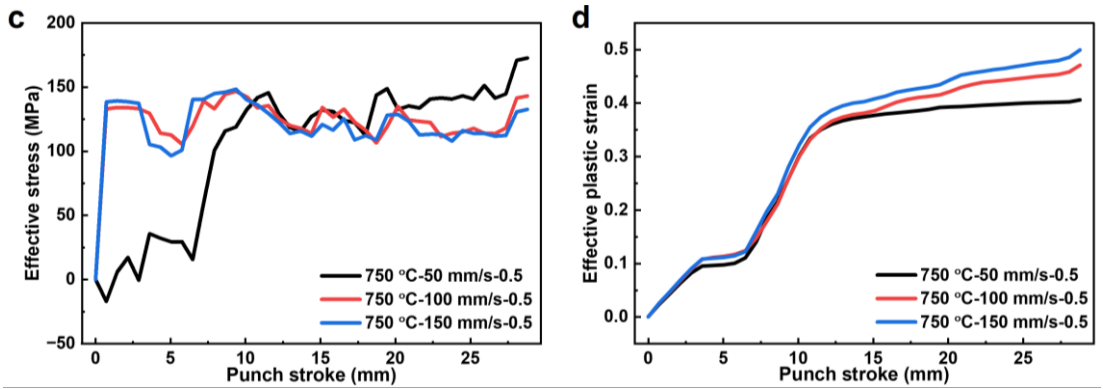


Figure 6. Effect of punch speed on the thermo-mechanical response and damage distribution at a die-entry temperature of 750 °C and a friction coefficient of 0.5: (a) 50 mm·s^{-1}; (b) 100 mm·s^{-1}; (c) 150 mm·s^{-1}

The histories at point P in Figure 7 further clarify this response. The final temperature increases from approximately 535 °C to 667 °C and 730 °C as the punch speed increases from 50 mm·s^{-1} to 100 mm·s^{-1} and 150 mm·s^{-1}, corresponding to temperature reductions of approximately 215 °C, 83 °C, and 20 °C, respectively. Meanwhile, the final effective stress decreases from approximately 173 MPa to 140 MPa and 135 MPa. Thus, higher punch speed simultaneously improves thermal retention and reduces the final effective stress. Conversely, the final effective plastic strain increases from approximately 0.41 to 0.47 and 0.50, while Damage increases from approximately 0.33 to 0.41 and 0.43. This contrasting response indicates that improved thermal retention and a lower final stress state do not necessarily lead to lower accumulated Damage.

This association between increased plastic deformation and damage accumulation is consistent with the damage-coupled viscoplastic model of Zhang *et al*. for 22MnB5 hot stamping, in which local necking and fracture damage are jointly governed by stress state, temperature, and strain rate that vary with location and forming history [29], and with the hot pre-deformation tests of Zhuang *et al*. on 22MnB5 at 850 °C, which showed that increasing forming strain raises the density of internal microvoids and microcracks and reduces failure strain and load-bearing capacity [30]. The increase in effective plastic strain and Damage under higher punch speeds is therefore interpreted primarily in terms of differences in the local thermo-mechanical forming history, rather than as a quantitatively validated strain-rate effect, given that the constitutive parameters were derived from flow-stress data at a nominal strain rate of 0.001 s^{-1} and were not independently validated over the broader strain-rate range considered here.



https://doi.org/10.64486/m.66.2.10

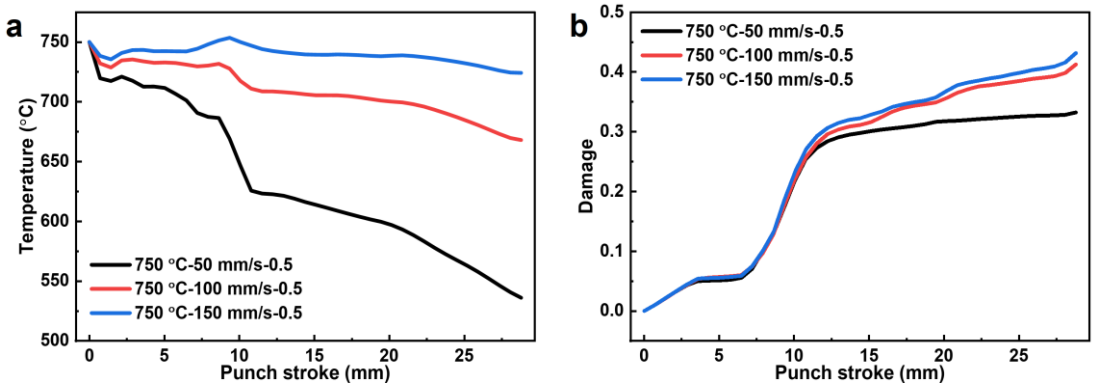


Figure 7. Evolution of temperature, Damage, effective stress, and effective plastic strain at point P with punch stroke under different punch speeds (50 mm·s^{-1}, 100 mm·s^{-1}, and 150 mm·s^{-1}) at a die-entry temperature of 750 °C and a friction coefficient of 0.5: (a) temperature; (b) Damage; (c) effective stress; (d) effective plastic strain

The friction coefficient produces a third characteristic response. Figure 8(a)–(c) presents the results for friction coefficients of 0.3, 0.5, and 0.7, respectively. Changing the friction coefficient does not substantially modify the location of the deformation-sensitive region. Its influence on the temperature field and effective stress distribution is also comparatively limited, whereas the high-effective-plastic-strain and high-Damage regions progressively broaden and become more continuous with increasing friction coefficient. This trend is further quantified at point P in Figure 9. The final temperature varies only slightly, from approximately 664 °C to 681 °C, and the effective stress remains within approximately (135–143) MPa, with no clear monotonic trend. In contrast, the final effective plastic strain increases progressively from 0.41 to 0.47 and 0.55, accompanied by an increase in Damage from 0.33 to 0.41 and 0.48 as the friction coefficient increases from 0.3 to 0.7.

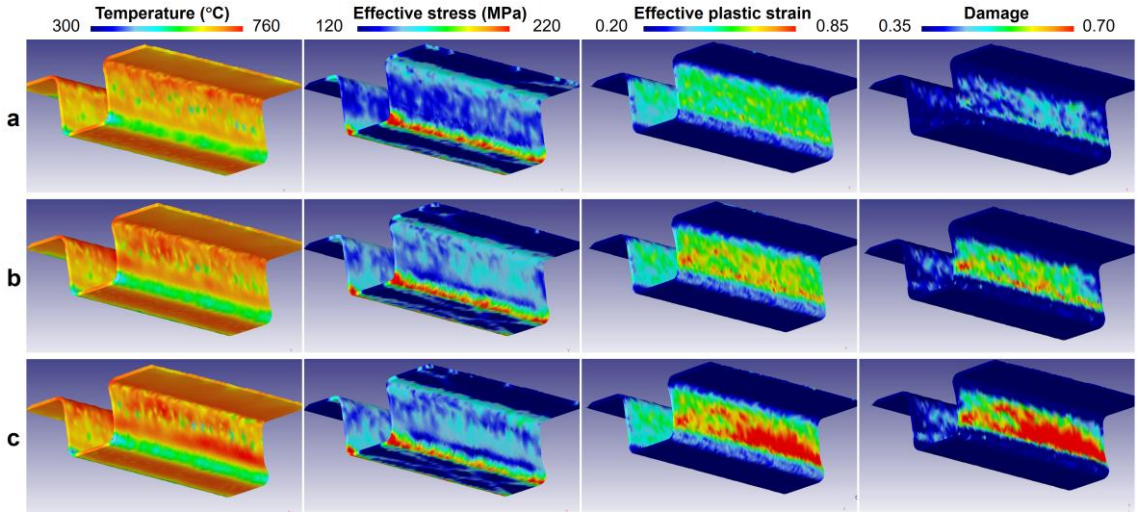


Figure 8. Effect of friction coefficient on the thermo-mechanical response and damage distribution of the 22MnB5 hot-stamped component at a die-entry temperature of 750 °C and a punch speed of 100 mm·s^{-1}: (a) 0.3; (b) 0.5; (c) 0.7

This behavior is consistent with the bending-under-tension (BUT) friction tests of He and Merklein on Al–Si-coated 22MnB5, in which sheet reorientation and sliding over a die radius—more representative of actual corner contact than flat-contact tests—showed friction to be jointly governed by corner radius, temperature, and coating condition [31], and with the thermo-mechanical-damage analysis of Hu *et al*., which indicated that friction affects the formability, damage evolution, and forming load of 22MnB5 sheet [20]. The absence of a monotonic trend in final effective stress is compatible with the continued increase in Damage: final stress reflects only the local state at the end of forming, whereas Damage accumulates over the entire stress–strain history, consistent with the view of Tekkaya *et al*. that forming damage should be regarded as a state

https://doi.org/10.64486/m.66.2.10

accumulated throughout deformation rather than one determined solely by the final stress [32]. The limited sensitivity of temperature and final effective stress, together with the monotonic increase in effective plastic strain and Damage, indicates that friction primarily modifies the local deformation response under the present conditions. The observed increase in effective plastic strain with friction is consistent with the increased interfacial constraint associated with higher friction [13], which may restrict relative sliding and material accommodation along the die surface under the constant-friction representation adopted in this model.

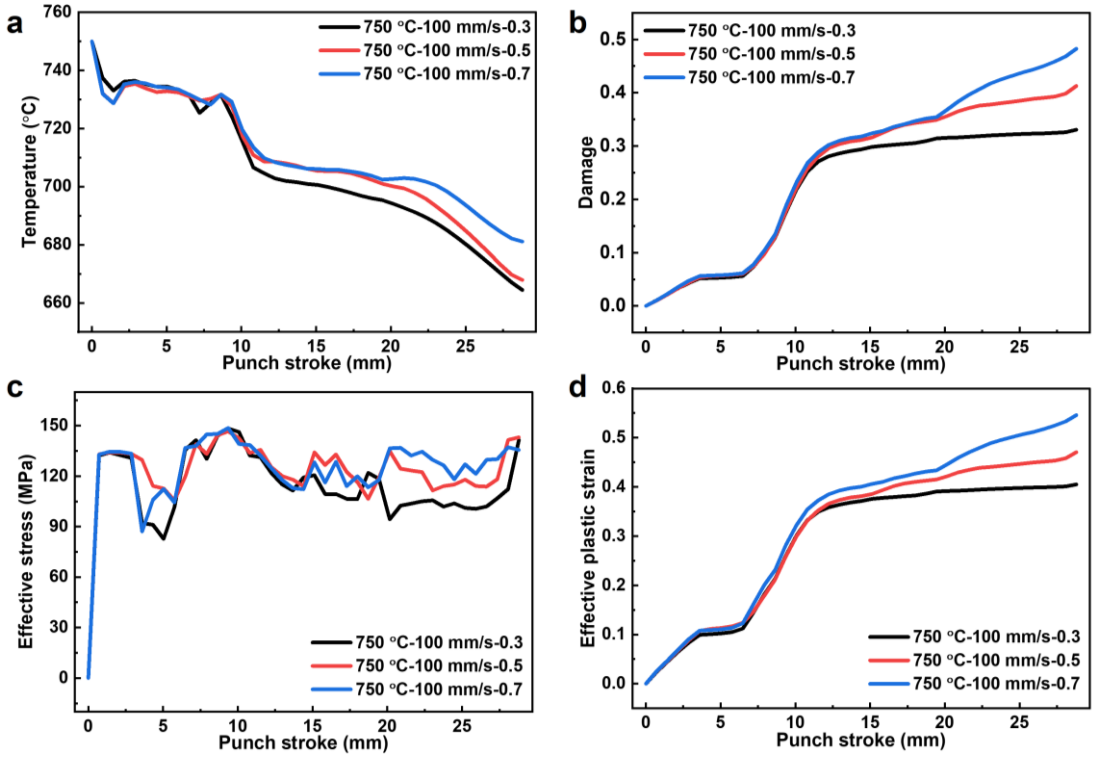


Figure 9. Evolution of temperature, Damage, effective stress, and effective plastic strain at point P with punch stroke under different friction coefficients (0.3, 0.5, and 0.7) at a die-entry temperature of 750 °C and a punch speed of 100 mm·s^{-1}: (a) temperature; (b) Damage; (c) effective stress; (d) effective plastic strain

The three single-factor groups reveal a common spatial characteristic but different response sensitivities. The high-effective-plastic-strain and high-Damage regions consistently remain concentrated in the mid-to-lower sidewall and sidewall–bottom-corner transition, indicating that the location of the deformation-sensitive region is relatively stable over the investigated process window. The process parameters mainly modify the magnitude of the local response rather than substantially relocating this region. Die-entry temperature primarily affects temperature and effective stress, whereas punch speed and friction coefficient produce stronger changes in effective plastic strain and Damage. Notably, punch speed links these two response tendencies by improving temperature retention and reducing effective stress while simultaneously increasing effective plastic strain and Damage. Thus, the single-factor results identify two distinct yet coupled response pathways: a thermal-softening pathway governing the local stress state and a deformation pathway associated with accumulated effective plastic strain and Damage. These observations provide the basis for examining whether the separation between instantaneous stress response and accumulated Damage is maintained when two process parameters vary concurrently in Section 3.2.

3.2. Responses under Two-Factor Process Variations

The single-factor results in Section 3.1 show that die-entry temperature primarily modifies the local stress level through thermal softening, whereas punch speed and friction coefficient have a stronger influence on accumulated plastic deformation and Damage. To examine whether these response characteristics are

https://doi.org/10.64486/m.66.2.10

maintained when two parameters vary concurrently, three representative two-factor groups, each comprising three selected parameter combinations, were investigated. Because these selected combinations do not constitute a full factorial design, the present simulations cannot isolate or quantitatively determine statistically identifiable interaction effects between the process parameters. Rather, they were used to compare the resulting thermo-mechanical and damage responses and determine whether the response pathways identified from the single-factor analysis remain consistent under representative concurrent process variations.

At a friction coefficient of μ = 0.5, Figure 10 compares three temperature–speed combinations: 750 °C–50 mm·s^{-1}, 800 °C–100 mm·s^{-1}, and 850 °C–150 mm·s^{-1}. Concurrent increases in die-entry temperature and punch speed improve thermal retention at point P. The final temperature increases from approximately 535 °C to 698 °C and 799 °C, due to the higher initial temperature and shorter forming time that limits heat transfer to the cooler die, while the corresponding effective stress decreases from approximately 173 MPa to 129 MPa and 115 MPa, reflecting the combined effects of temperature and punch speed, with the latter also affecting the local strain-rate history. Despite this reduction in effective stress, Damage increases from approximately 0.33 to 0.38 and 0.43, accompanied by an increase in effective plastic strain from approximately 0.41 to 0.44 and 0.50. Lennemann *et al*. reported that, under controlled forming conditions, higher temperature can reduce microvoid formation and increase subsequent fracture strain [33]. Because die-entry temperature alone produced little change in final Damage in Section 3.1, the increase observed here is more plausibly associated with the concurrent increase in punch speed, consistent with its stronger influence on accumulated deformation. Damage increases mainly within a punch-stroke range of approximately (8–12) mm under all three conditions.

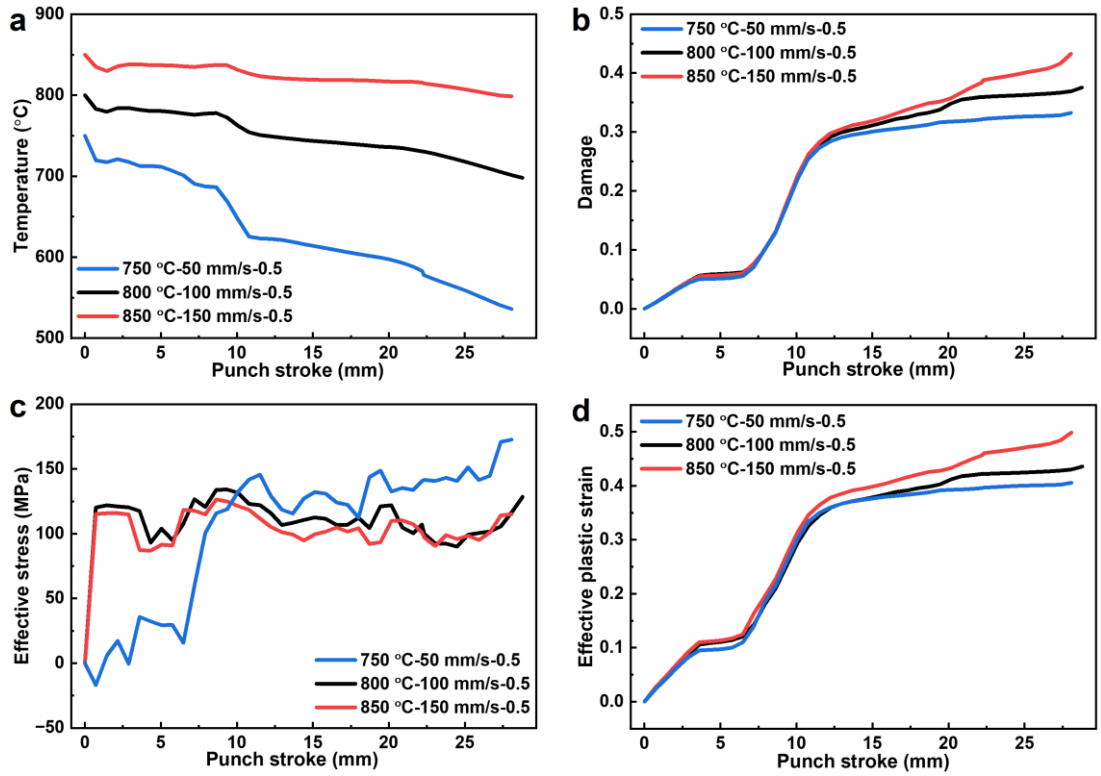


Figure 10. Evolution of temperature, Damage, effective stress, and effective plastic strain at point P with punch stroke under different die-entry temperature–punch speed combinations (750 °C–50 mm·s^{-1}, 800 °C–100 mm·s^{-1}, and 850 °C–150 mm·s^{-1}) at a friction coefficient of 0.5: (a) temperature; (b) Damage; (c) effective stress; (d) effective plastic strain

Given the geometric transition at this location, this stroke range plausibly coincides with the stage where the blank undergoes contact-state change and flow reorientation at the sidewall–bottom-corner transition, although this was not independently verified through contact-area or flow-direction data in the present model. The temperature–speed combinations mainly alter the increment and final magnitude of strain and Damage

 https://doi.org/10.64486/m.66.2.10

within this stage, rather than the punch-stroke range over which rapid accumulation occurs. This is qualitatively consistent with He *et al.*'s report that higher punch speed widens the effective plastic strain-rate difference among deformation zones in 22MnB5 hot stamping, promoting more non-uniform local deformation [27]. These results indicate that the temperature–speed combinations retain the same response pathway as in the single-factor analysis: improved thermal retention and reduced effective stress are accompanied by increased effective plastic strain and Damage, driven primarily by punch speed rather than by die-entry temperature.

Having examined the temperature–speed coupling, we next consider friction as the second coupled variable. At a fixed punch speed of 100 mm·s^{-1}, Figure 11 compares three temperature–friction combinations: 750 °C–μ = 0.3, 800 °C–μ = 0.5, and 850 °C–μ = 0.7. As both die-entry temperature and friction coefficient increase concurrently, the final temperature at point P increases from approximately 664 °C to 698 °C and 738 °C, whereas effective stress decreases from approximately 141 MPa to 129 MPa and 123 MPa. In contrast, effective plastic strain and Damage increase substantially over the same range, from 0.41 to 0.44 and 0.49 and from 0.33 to 0.38 and 0.43, respectively. As with the temperature–speed group, this increase is more plausibly attributed to friction than temperature, since temperature alone was shown in Section 3.1 to produce little change in Damage — consistent with the coupled thermal–friction behavior reported for coated 22MnB5 blanks [34].

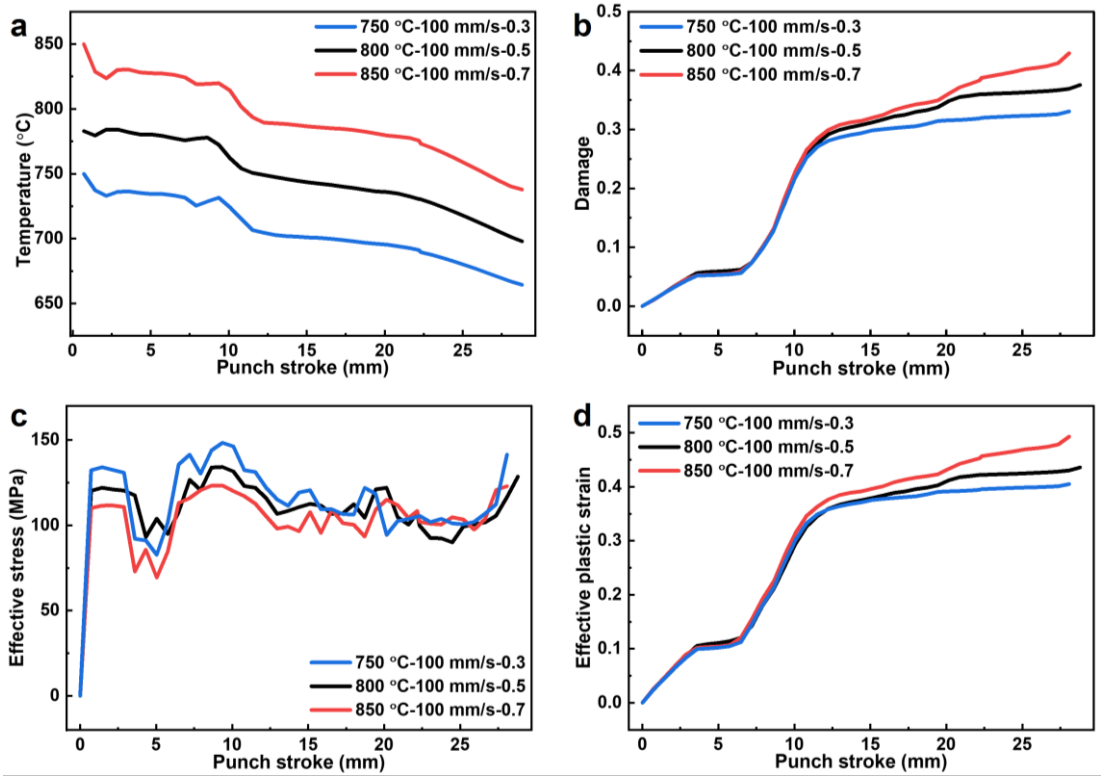


Figure 11. Evolution of temperature, Damage, effective stress, and effective plastic strain at point P with punch stroke under different die-entry temperature–friction coefficient combinations (750 °C–0.3, 800 °C–0.5, and 850 °C–0.7) at a punch speed of 100 mm·s^{-1}: (a) temperature; (b) Damage; (c) effective stress; (d) effective plastic strain

The third combination examines the concurrent effects of punch speed and friction at a fixed die-entry temperature of 800 °C. Figure 12 compares three speed–friction combinations: 50 mm·s^{-1}–μ = 0.3, 100 mm·s^{-1}–μ = 0.5, and 150 mm·s^{-1}–μ = 0.7, which produce the largest increase in Damage among the three coupled groups. As both parameters increase, the final temperature rises from approximately 572 °C to 698 °C and 770 °C, effective stress decreases from approximately 164 MPa to 129 MPa and 118 MPa, effective plastic strain increases from 0.38 to 0.44 and 0.58, and Damage increases from 0.30 to 0.38 and 0.53. This is consistent with the same stress–Damage decoupling pathway, reflecting the combined influence of two parameters both individually shown in Section 3.1 to strongly affect accumulated deformation. In practical hot stamping, punch speed and friction are not fully independent, as contact pressure, sliding velocity, and surface conditions jointly affect

https://doi.org/10.64486/m.66.2.10

interfacial behavior [35], which may further amplify the response observed here.

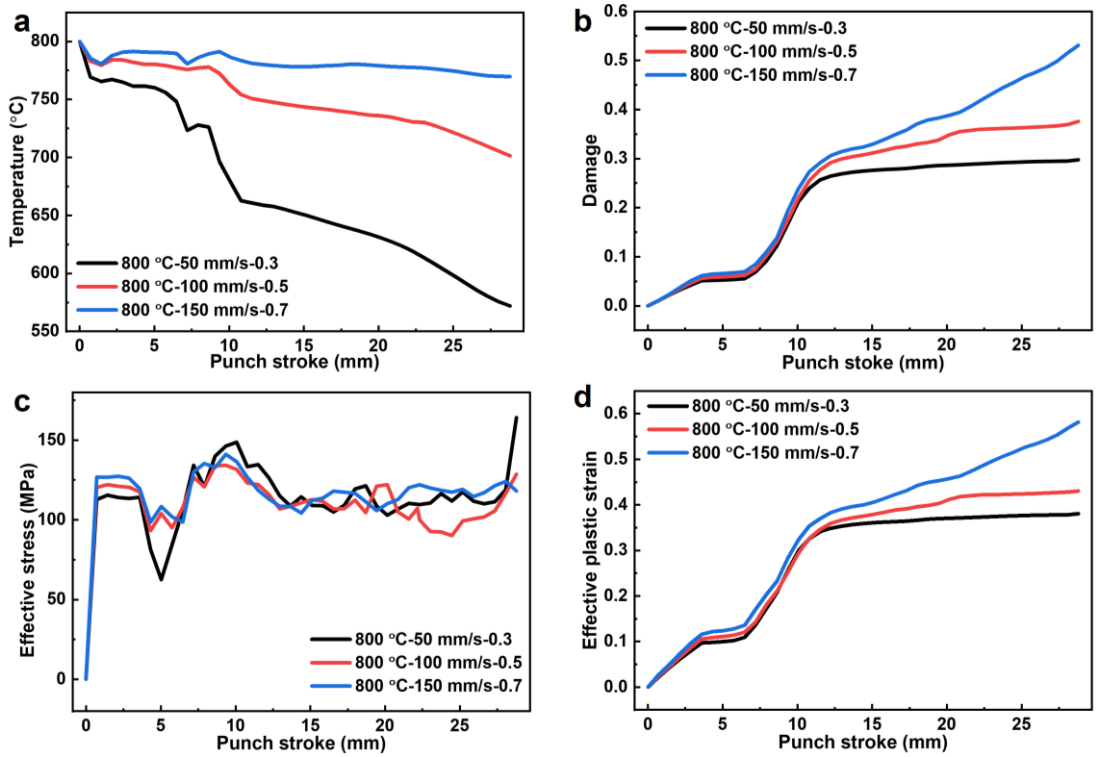


Figure 12. Evolution of temperature, Damage, effective stress, and effective plastic strain at point P with punch stroke under different punch speed–friction coefficient combinations (50 mm·s^{-1}–0.3, 100 mm·s^{-1}–0.5, and 150 mm·s^{-1}–0.7) at a die-entry temperature of 800 °C: (a) temperature; (b) Damage; (c) effective stress; (d) effective plastic strain

To further quantify these trends across all investigated conditions, the final effective plastic strain, effective stress, and Damage at point P were compiled across 12 unique simulation conditions (n = 12), spanning the single- and two-factor simulations and comprising all non-overlapping cases from the three single-factor and three two-factor groups. As shown in Figure 13, within the investigated process window, final Damage exhibits a strong, approximately linear relationship with final effective plastic strain (R^2 = 0.99, p < 0.001, n = 12), whereas final Damage shows a weaker correlation with final effective stress (R^2 = 0.62, p ≈ 0.0023, n = 12). Because both regressions are based on a relatively small number of simulation conditions, these statistical relationships should be interpreted with appropriate caution, particularly for the Damage–effective stress relationship in Figure 13(b). Several low-stress conditions are nevertheless associated with relatively high Damage values. This comparison provides quantitative support for the response pattern observed in the individual and coupled simulations. The strong Damage–effective plastic strain correlation should, however, be interpreted in light of the NCL formulation, in which accumulated plastic strain directly contributes to the Damage integral; therefore, the high R^2 value does not by itself constitute independent evidence of a causal physical relationship. This difference can be understood from the distinct physical meanings of the two quantities. Effective stress represents the instantaneous mechanical state and is strongly affected by temperature-dependent thermal softening; in the present study, its sensitivity to interfacial friction is comparatively limited (Section 3.1). In contrast, effective plastic strain and the NCL Damage index retain the effects of the preceding deformation history. Chen *et al*. showed for high-temperature NCL-type modeling that damage prediction depends not only on accumulated plastic strain but also on temperature, strain rate, and the calibration procedure used for the model parameters [36]. Tarhouni *et al.* further noted that, even at a comparable level of plastic strain, damage initiation and evolution still vary with stress triaxiality and the Lode parameter — factors not evaluated in the present study [37]. The residual scatter in the Damage–effective plastic strain relationship may also reflect differences in the local stress-state path during forming. Consequently, the local stress level may decrease as

https://doi.org/10.64486/m.66.2.10

temperature increases, while accumulated effective plastic strain and Damage continue to increase under conditions that promote greater deformation. Within the investigated process window and the present NCL framework, effective plastic strain shows a stronger association with the final Damage response than effective stress, whereas effective stress alone does not fully characterize the accumulated Damage level.

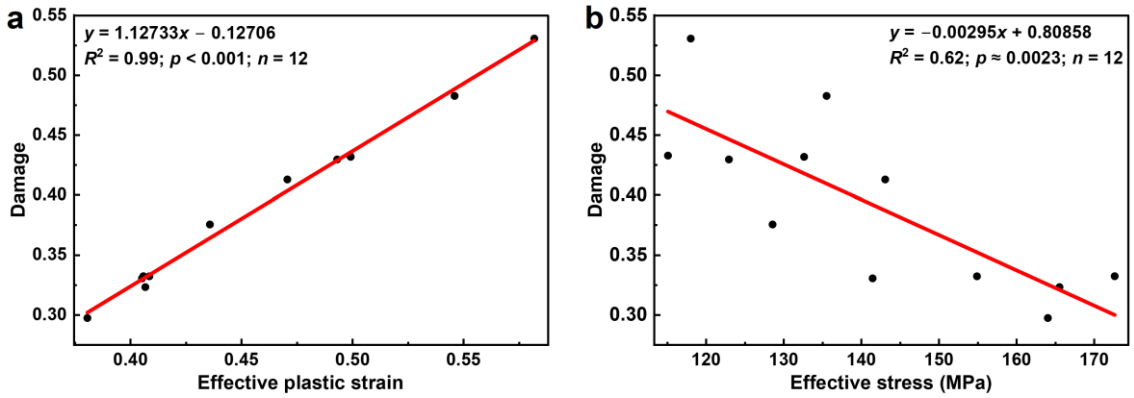


Figure 13. Relationships between final Damage and (a) final effective plastic strain and (b) final effective stress at point P, across 12 unique simulation conditions. Linear regression results (equation, R^2, and p-value) are given within each panel

As a cross-check across the three two-factor groups, their shared central condition (800 °C–100 mm·s^{-1}–μ = 0.5) was compared. At this condition, the final temperature, effective stress, effective plastic strain, and Damage at point P are approximately 698 °C, (128–129) MPa, 0.44, and 0.38, respectively, across the three groups, with Damage varying only slightly (0.376–0.380) among the groups. The close agreement among these values provides an internal consistency check for the extraction and comparison of the simulated response histories. Taken together, the coupled simulations support the response pathways identified in Section 3.1: die-entry temperature primarily modifies the thermal state and effective stress, whereas punch speed and friction have stronger effects on accumulated effective plastic strain and Damage. The deformation-sensitive region remains spatially stable, while the process parameters mainly determine the magnitude of its local deformation and Damage response. Although direct experimental validation was not performed, previous studies have reported localized thinning and/or cracking in geometrically constrained regions of hot-stamped 22MnB5 components, including sidewall and beam-type regions [4,5,11,38]. These observations provide qualitative contextual support for the predicted localization of deformation and damage in the present geometry, but do not constitute quantitative validation because of differences in geometry, forming conditions, material state, and damage formulation. Accordingly, the NCL Damage parameter is used here as a dimensionless relative indicator for comparing damage evolution among process conditions rather than as a quantitatively calibrated crack-initiation criterion.

4. Conclusions

A thermo-mechanically coupled finite element model of 22MnB5 hot-stamp bending was established in DEFORM-3D to investigate temperature, effective stress, effective plastic strain, and NCL Damage in the sidewall–bottom-corner transition region under variations in die-entry temperature, punch speed, and friction coefficient. The main conclusions are as follows:

(1) The deformation-sensitive region remained spatially stable, with high effective plastic strain and Damage consistently localized in the mid-to-lower sidewall and sidewall–bottom-corner transition. Increasing the die-entry temperature from 750 °C to 850 °C primarily reduced effective stress through thermal softening, while the final effective plastic strain (≈0.41) and Damage (≈0.32 to 0.33) remained nearly unchanged.

(2) Punch speed and friction coefficient produced stronger changes in accumulated plastic deformation and Damage than in the final thermal and stress states. Increasing punch speed from 50 mm·s^{-1} to 150 mm·s^{-1} improved temperature retention and reduced effective stress from approximately 173 MPa to 135 MPa, while

https://doi.org/10.64486/m.66.2.10

increasing the final effective plastic strain (≈0.41 to 0.50) and Damage (≈0.33 to 0.43). Increasing the friction coefficient from 0.3 to 0.7 had limited effects on temperature and stress but substantially increased the final effective plastic strain (≈0.41 to 0.55) and Damage (≈0.33 to 0.48). These results indicate that process parameters can alter Damage accumulation primarily through their influence on the deformation history.

(3) Across the 12 unique simulation conditions, final Damage showed a strong approximately linear correlation with final effective plastic strain (R^2 = 0.99), whereas its relationship with final effective stress was weaker and more scattered (R^2 = 0.62). The high Damage–effective plastic strain correlation should be interpreted in light of the NCL formulation, which computes Damage by integrating stress-related terms over accumulated plastic strain and therefore inherently links the two quantities; consequently, the high R^2 does not by itself establish an independent causal relationship.

Overall, the results show that instantaneous stress and accumulated Damage may follow different process-dependent trends in the sidewall–bottom-corner transition region. Thermal softening can reduce instantaneous stress without necessarily reducing accumulated Damage because Damage depends on both the evolving stress state and deformation history. The present results should therefore be interpreted as mechanistic trends rather than quantitative predictions of cracking, given the relative nature of the NCL Damage indicator, limited independent strain-rate validation, constant friction and tooling conditions, and the use of selected rather than full-factorial two-factor combinations. Experimental validation, including thickness evolution and relevant surface/coating effects, would be needed for quantitative assessment of cracking behavior.

Acknowledgments: This work was supported by the Advanced Materials-National Science and Technology Major Project (2025ZD0611100).

References

[1] I. Wróbel, A. Skowronek, and A. Grajcar, "A review on hot stamping of advanced high-strength steels: Technological-metallurgical aspects and numerical simulation," *Symmetry*, vol. 14, no. 5, Art. no. 969, 2022, https://doi.org/10.3390/sym14050969

[2] H. Karbasian and A. E. Tekkaya, "A review on hot stamping," *Journal of Materials Processing Technology*, vol. 210, no. 15, pp. 2103–2118, 2010, https://doi.org/10.1016/j.jmatprotec.2010.07.019

[3] H. Sun, S. Yao, Q. Tang, R. Rong, G. Chu, P. Auer, and J. Domitner, "Short-wave infrared heating of 22MnB5 steel with adjusted surface emissivity for press hardening of tailored-strength components," *Journal of Manufacturing Processes*, vol. 120, pp. 74–85, 2024, https://doi.org/10.1016/j.jmapro.2024.04.032

[4] H. Y. Seo, C. K. Jin, and C. G. Kang, "Effect on blank holding force on blank deformation at direct and indirect hot deep drawings of boron steel sheets," *Metals*, vol. 8, no. 8, Art. no. 574, 2018, https://doi.org/10.3390/met8080574

[5] Z. Tang, Z. Gu, Y. Li, X. Li, G. Yu, and L. Yi, "Study on the effect of the pre-forming of 22MnB5 steel in indirect hot stamping," *Materials*, vol. 16, no. 10, Art. no. 3739, 2023, https://doi.org/10.3390/ma16103739

[6] A. Turetta, S. Bruschi, and A. Ghiotti, "Investigation of 22MnB5 formability in hot stamping operations," *Journal of Materials Processing Technology*, vol. 177, no. 1–3, pp. 396–400, 2006, https://doi.org/10.1016/j.jmatprotec.2006.04.041

[7] M. Merklein and J. Lechler, "Investigation of the thermo-mechanical properties of hot stamping steels," *Journal of Materials Processing Technology*, vol. 177, no. 1–3, pp. 452–455, 2006, https://doi.org/10.1016/j.jmatprotec.2006.03.233

[8] P. Åkerström and M. Oldenburg, "Austenite decomposition during press hardening of a boron steel—Computer simulation and test," *Journal of Materials Processing Technology*, vol. 174, no. 1–3, pp. 399–406, 2006, https://doi.org/10.1016/j.jmatprotec.2006.02.013

[9] C. P. Couto, R. I. Revilla, R. Politano, I. Costa, Z. Panossian, I. D. Graeve, J. L. Rosso, and H. Terryn, "Influence of austenitisation temperatures during hot stamping on the local electrochemical behaviour of 22MnB5 steel coated with hot-dip Al-Si," *Corrosion Science*, vol. 190, Art. no. 109673, 2021, https://doi.org/10.1016/j.corsci.2021.109673

[10] T. Maeno, K. Mori, and T. Nagai, "Improvement in formability by control of temperature in hot stamping of ultra-high strength steel parts," *CIRP Annals*, vol. 63, no. 1, pp. 301–304, 2014, https://doi.org/10.1016/j.cirp.2014.03.005

[11] J. Cui, G. Sun, J. Xu, X. Huang, and G. Li, "A method to evaluate the formability of high-strength steel in hot stamping," *Materials & Design*, vol. 77, pp. 95–109, 2015, https://doi.org/10.1016/j.matdes.2015.04.009

 https://doi.org/10.64486/m.66.2.10

[12] A. Ghiotti, S. Bruschi, and F. Borsetto, "Tribological characteristics of high strength steel sheets under hot stamping conditions," *Journal of Materials Processing Technology*, vol. 211, no. 11, pp. 1694–1700, 2011, https://doi.org/10.1016/j.jmatprotec.2011.05.009

[13] A. Yanagida and A. Azushima, "Evaluation of coefficients of friction in hot stamping by hot flat drawing test," *CIRP Annals*, vol. 58, no. 1, pp. 247–250, 2009, https://doi.org/10.1016/j.cirp.2009.03.091

[14] A. Azushima, K. Uda, and A. Yanagida, "Friction behavior of aluminum-coated 22MnB5 in hot stamping under dry and lubricated conditions," *Journal of Materials Processing Technology*, vol. 212, no. 5, pp. 1014–1021, 2012, https://doi.org/10.1016/j.jmatprotec.2011.12.009

[15] J. Hardell, E. Kassfeldt, and B. Prakash, "Friction and wear behaviour of high strength boron steel at elevated temperatures of up to 800 °C," *Wear*, vol. 264, no. 9–10, pp. 788–799, 2008, https://doi.org/10.1016/j.wear.2006.12.077

[16] L. Pelcastre, J. Hardell, A. Rolland, and B. Prakash, "Influence of microstructural evolution of Al-Si coated UHSS on its tribological behaviour against tool steel at elevated temperatures," *Journal of Materials Processing Technology*, vol. 228, pp. 117–124, 2016, https://doi.org/10.1016/j.jmatprotec.2015.03.009

[17] J. Min, J. Lin, J. Li, and W. Bao, "Investigation on hot forming limits of high strength steel 22MnB5," *Computational Materials Science*, vol. 49, no. 2, pp. 326–332, 2010, https://doi.org/10.1016/j.commatsci.2010.05.018

[18] T. Wierzbicki, Y. Bao, Y.-W. Lee, and Y. Bai, "Calibration and evaluation of seven fracture models," *International Journal of Mechanical Sciences*, vol. 47, no. 4–5, pp. 719–743, 2005, https://doi.org/10.1016/j.ijmecsci.2005.03.003

[19] C. W. Lee, D. W. Fan, I. R. Sohn, S.-J. Lee, and B. C. De Cooman, "Liquid-metal-induced embrittlement of Zn-coated hot stamping steel," *Metallurgical and Materials Transactions A*, vol. 43, no. 13, pp. 5122–5127, 2012, https://doi.org/10.1007/s11661-012-1316-0

[20] P. Hu, D. Shi, L. Ying, G. Shen, and W. Liu, "The finite element analysis of ductile damage during hot stamping of 22MnB5 steel," *Materials & Design*, vol. 69, pp. 141–152, 2015, https://doi.org/10.1016/j.matdes.2014.12.044

[21] J. Zhou, Y. Mu, and B. Wang, "A damage-coupled unified viscoplastic constitutive model for prediction of forming limits of 22MnB5 at high temperatures," *International Journal of Mechanical Sciences*, vol. 133, pp. 457–468, 2017, https://doi.org/10.1016/j.ijmecsci.2017.09.006

[22] B. Tang, F. Wu, Q. Wang, J. Liu, N. Guo, H. Ge, Q. Wang, and P. Liu, "Damage prediction of hot stamped boron steel 22MnB5 with a microscopic motivated ductile fracture criterion: Experiment and simulation," *International Journal of Mechanical Sciences*, vol. 169, Art. no. 105302, 2020, https://doi.org/10.1016/j.ijmecsci.2019.105302

[23] J. Venema, J. Hazrati, E. Atzema, D. Matthews, and T. van den Boogaard, "Multiscale friction model for hot sheet metal forming," *Friction*, vol. 10, no. 2, pp. 316–334, 2022, https://doi.org/10.1007/s40544-021-0504-6

[24] J. Zhou, B. Wang, and M. Huang, "Two constitutive descriptions of boron steel 22MnB5 at high temperature," *Materials & Design*, vol. 63, pp. 738–748, 2014, https://doi.org/10.1016/j.matdes.2014.07.008

[25] J. Tungtrongpairoj, V. Uthaisangsuk, and W. Bleck, "Determination of yield behaviour of boron alloy steel at high temperature," *Journal of Metals, Materials and Minerals*, vol. 19, no. 1, pp. 29–38, 2009, https://jmmm.material.chula.ac.th/index.php/jmmm/article/view/220/247

[26] R. Zhang, Z. Shi, V. A. Yardley, and J. Lin, "Experimental studies of necking and fracture limits of boron steel sheet under hot stamping conditions," *Journal of Materials Processing Technology*, vol. 302, Art. no. 117481, 2022, https://doi.org/10.1016/j.jmatprotec.2021.117481

[27] W. He, B. Yang, X. Zhang, M. Li, S. Sun, B. Wang, and Q. Ma, "Investigation into the hot-forming limit for 22MnB5 hot-forming steel under a stamping process," *Metals*, vol. 14, no. 5, Art. no. 561, 2024, https://doi.org/10.3390/met14050561

[28] M. Ganapathy, N. Li, J. Lin, M. Abspoel, and D. Bhattacharjee, "Experimental investigation of a new low-temperature hot stamping process for boron steels," *The International Journal of Advanced Manufacturing Technology*, vol. 105, no. 1–4, pp. 669–682, 2019, https://doi.org/10.1007/s00170-019-04172-5

[29] R. Zhang, Z. Shi, V. A. Yardley, and J. Lin, "A CDM-based unified viscoplastic constitutive model of FLCs and FFLCs for boron steel under hot stamping conditions," *International Journal of Damage Mechanics*, vol. 31, no. 9, pp. 1373–1395, 2022, https://doi.org/10.1177/10567895221105655

[30] W. Zhuang, P. Wang, D. Xie, and H. Shi, "Experimental study and a damage model approach to determine the effect of hot forming deformation on the service performance of 22MnB5 steel," *Journal of Manufacturing Processes*, vol. 47,

pp. 10–21, 2019, https://doi.org/10.1016/j.jmapro.2019.09.018

[31] F. He and M. Merklein, "Investigation of the tribological behaviour of hot stamping steel in a bending-under-tension test," *Wear*, vol. 593, Art. no. 206583, 2026, https://doi.org/10.1016/j.wear.2026.206583

[32] A. E. Tekkaya, P.-O. Bouchard, S. Bruschi, and C. C. Tasan, "Damage in metal forming," *CIRP Annals*, vol. 69, no. 2, pp. 600–623, 2020, https://doi.org/10.1016/j.cirp.2020.05.005

[33] P. Lennemann, A. E. Tekkaya, and Y. P. Korkolis, "Influence of forming temperature on damage and product performance in hot stamping of steel," in *Proc. 28th Int. ESAFORM Conf. on Material Forming (ESAFORM 2025)* (*Materials Research Proceedings*, vol. 54), Paestum, Italy, 2025, pp. 1249–1256, https://doi.org/10.21741/9781644903599-136

[34] M.-K. Ji, H. S. Son, J. K. Oh, S. W. Kim, F. Alkelae, and T.-S. Jun, "Effects of heat treatment on tribological behaviour of Al–Si coated 22MnB5 and SKD61 tool steels in hot stamping," *Metals and Materials International*, vol. 31, no. 7, pp. 1949–1961, 2025, https://doi.org/10.1007/s12540-024-01862-y

[35] P. Schwingenschlögl and M. Merklein, "Characterization of tribological conditions within direct hot stamping," *Journal of Materials Processing Technology*, vol. 278, Art. no. 116535, 2020, https://doi.org/10.1016/j.jmatprotec.2019.116535

[36] X. Chen, Y. Mao, Z. Zhou, L. Sun, S. Zhao, and Z. Yang, "Parameter identification of normalized Cockcroft & Latham elevated temperature damage model for 35CrMo steel using inverse optimization method," *Materials Today Communications*, vol. 42, Art. no. 111210, 2025, https://doi.org/10.1016/j.mtcomm.2024.111210

[37] I. Tarhouni, P. Maimí, D. Frómeta, and D. Casellas, "Modelling of ductile fracture considering the effect of stress triaxiality and the energy partition theory in thin high-strength steel sheets," *International Journal of Fracture*, vol. 249, no. 2, Art. no. 24, 2025, https://doi.org/10.1007/s10704-025-00844-4

[38] Y. Chang, S. Li, X. Li, C. Wang, P. Hu, and K. Zhao, "Effect of contact pressure on IHTC and the formability of hot-formed 22MnB5 automotive parts," *Applied Thermal Engineering*, vol. 99, pp. 419–428, 2016, https://doi.org/10.1016/j.applthermaleng.2016.01.053